

Inland lake temperature initialization via coupled cycling with atmospheric data assimilation

Stanley G. Benjamin¹, Tatiana G. Smirnova^{2,1}, Eric P. James^{2,1}, Eric J. Anderson³, Ayumi Fujisaki-Manome^{4,5}, John G.W. Kelley⁶, Greg E. Mann⁷, Andrew D. Gronewold⁵, Philip Chu⁸, Sean G.T. Kelley⁹

¹NOAA Global Systems Laboratory, Boulder, CO 80305 USA

²Cooperative Institute for Research in Environmental Science (CIRES), University of Colorado, Boulder, CO 80303 USA

³Civil and Engineering Department, Colorado School of Mines, Golden, CO USA

⁴Cooperative Institute for Great Lakes Research (CIGLR), University of Michigan, Ann Arbor, MI USA

⁵University of Michigan, Ann Arbor, MI USA

⁶NOAA National Ocean Service, Coast Survey Development Laboratory, Durham, NH 03824 USA

⁷NOAA National Weather Service, White Lake, MI, USA

⁸NOAA Great Lakes Environmental Research Laboratory, Ann Arbor, MI, USA

⁹University of Massachusetts, Department of Mathematics and Statistics, Amherst, MA, USA

Correspondence to: [Tatiana Smirnova \(tanya.smirnova@noaa.gov\)](mailto:tanya.smirnova@noaa.gov)

8 Dec 2021 - submitted to Geoscientific Model Development (GMD)

https://gmd.copernicus.org/articles/special_issue1114.html

Special issue I Modelling inland waters in a changing climate (GMD/ESD/TC inter-journal SI).

- Resubmitted with editorial changes – 21 Jan 2022, 21 June 2022, 28 July 2022

Abstract. Application of lake models coupled within earth-system prediction models, especially for predictions from days to weeks, requires accurate initialization of lake temperatures. Commonly used methods to initialize lake temperatures include interpolation of global SST analyses to inland lakes, daily satellite-based observations or model-based re-analyses. However, each of these methods have limitations in capturing the temporal characteristics of lake temperatures (e.g., effects of anomalously warm or cold weather) for all lakes within a geographic region, and/or during extended cloudy periods. An alternative lake initialization method was developed which uses 2-way coupled cycling of a small-lake model within an hourly data assimilation system of a weather prediction model. The lake model simulated lake temperatures were compared with other estimates from satellite and in-situ observations and interpolated-SST data for a multi-month period in 2021. The lake cycling initialization, now applied to two operational US NOAA weather models, was found to decrease errors in lake surface temperature from as much as 5-10 K vs. interpolated-SST data to about 1-2 K compared to available in-situ and satellite observations.

Deleted: Stan Benjamin (stan.benjamin)

Deleted: short-term

Deleted: Here, we describe a

Deleted: by

Deleted: updated

Deleted: to constrain lake temperature evolution. We compare these ...

Deleted: temperature values

Deleted:

Deleted: sets

Deleted: 10K (using

Deleted:)

Deleted: (comparing with

Deleted:

Short summary

Application of 1-d lake models coupled within earth-system prediction models will improve accuracy but requires accurate initialization of lake temperatures. Here, we describe a lake initialization method by coupled cycling within a weather prediction model to constrain lake temperature evolution. We compare these lake temperature values with other estimates and found much reduced errors (down to 1-2 K). The lake cycling initialization is now applied to two operational US NOAA weather models.

1 Introduction

Inclusion of lake representation into numerical weather prediction (NWP) models has become increasingly necessary to further improve representation of atmosphere-surface fluxes of heat and moisture as model grid resolution becomes finer. Representation of lake physics to provide time-varying lake surface properties (e.g., Subin et al, 2012) is essential to improve fluxes of heat, moisture and momentum between the surface and atmosphere (Hostetler et al, 1993, Thiery et al, 2014). Lake representation is part of the overall surface treatment including land-surface models (LSMs) necessary to accurately model the evolution of the planetary boundary layer, ~~in the atmosphere~~. Lakes are estimated to cover 3.7% of the global non-glaciated land area (Verpoorter et al, 2014), and they significantly moderate sensible heat and moisture fluxes from this 'land' (i.e., non-ocean) area. Water impoundments (reservoirs) that used to account for about 6% of these 'lake' areas (Downing et al, 2006) have recently increased to 9% (Vanderkelen et al, 2021). Initial conditions for both land and lake surface are an important consideration due to far larger thermal inertia for soil or water than for air. Consequently, incorrect soil or lake initial conditions can result in erroneous heat and moisture fluxes that may persist for days and even weeks (e.g., Dirmeyer et al, 2018). This potential source of error in fluxes is more pronounced for lake areas with far larger thermal inertia and heat storage than even saturated soils.

In operational US NOAA weather prediction models (global and regional) up to this point, daily sea-surface temperature (SST) analyses have been used to specify the surface water temperatures for even small inland lakes. Inland lake temperatures in North America have been obtained by the interpolation of SST values from the ocean and the Laurentian Great Lakes. An alternative is to incorporate one-dimensional (1-d) lake models within NWP models and use ~~a continuous lake simulation~~ forced by atmospheric conditions updated ~~regularly~~ by new ~~atmospheric~~ observations ~~to obtain~~ realistic lake water temperatures (e.g., "cycling"). This cycling to initialize small lakes in NOAA operational regional weather prediction models complements loose coupling with a 3-d hydrodynamical lake model for the Laurentian Great Lakes as described elsewhere in Fujisaki-Manome et al 2020.

Deleted: .

Deleted: coupled cycling

Deleted: and continuously simulated 1-d lake models

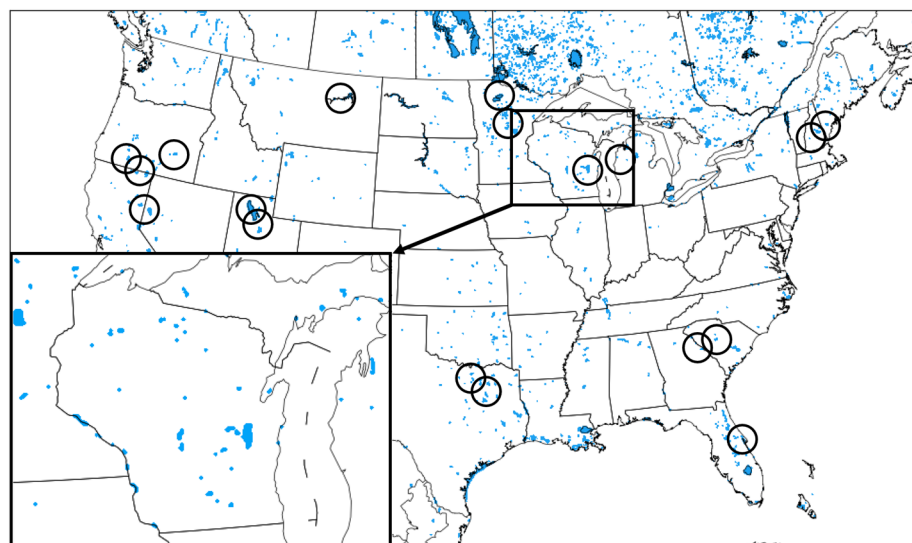
Lake representation (via one-dimensional (1-d) models, as in LSMs) within NWP models is beneficial by providing a first-order accurate lagged effect of the seasonal variation in temperature, with lake water remaining colder than nearby land in spring and warmer in autumn. The outcomes are desirable, as described by Balsamo et al (2012), for instance by accurately representing increased evaporative fluxes in the fall. Thus, use of a 1-d lake model has the potential to improve over land representation by capturing this slower seasonal response.

However, lake temperature initialization from SST (e.g., Mallard et al, 2015) can exaggerate this seasonal slower response. Shallow lakes warm more slowly in spring than surrounding land, but more quickly than nearby deeper lakes. Even in summer, it will take at least 1-2 weeks for cycled 1-d models to adjust from values interpolated from deeper-lake temperatures to become more realistic for shallow lakes. Therefore, lake temperature initialization becomes the most important factor to accurately simulate sensible and latent heat fluxes from lakes for short to medium-range NWP, more so than the use of the lake model itself. One option to solve the lake initialization problem is to use a model-based climatology for seasonal variation of lake temperatures (Balsamo et al (2012) and Balsamo (2013), ECMWF) using a 1-d lake model forced by reanalysis data. The 1-d lake model used by ECMWF for this method is the 2-layer FLake (Freshwater Lake Model) model (Mironov et al, 2010, Balsamo et al, 2012, Boussetta et al, 2021) and also implemented into their Integrated Forecast System (IFS) in 2015. A similar technique was applied by Mironov et al (2010) using FLake for the COSMO model. Kourzeneva et al (2012a) describe application of 20-year reanalysis data to create a global lake climatology dataset using FLake. This technique avoids a new spin-up with each new run, but cannot capture unique weather regime variations in a given region and time. The UK Met Office uses satellite data to update their lake surface water temperatures using the previous day values as a background (Fiedler et al, 2014). Another option to solve the lake initialization problem, described here, is lake temperature evolution, referred to as “lake cycling”, with the ongoing 1-d lake prediction within an NWP model, a cost-free option if the atmospheric conditions are relatively accurate.

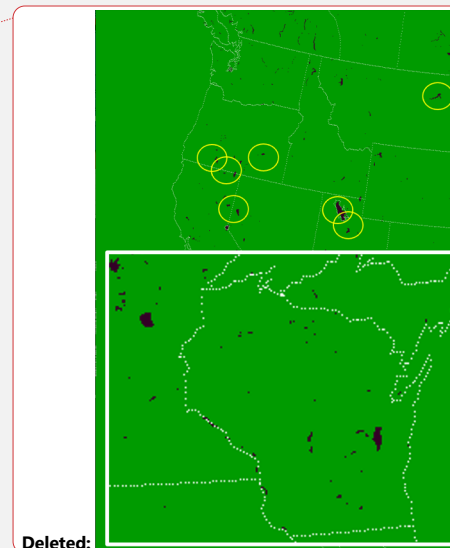
Data assimilation for land-surface fields (e.g., soil temperature, soil moisture, snow cover, snow water equivalent, snow temperature) has been very beneficial for improved short-range weather prediction accuracy (e.g., Balsamo and Mahfouf, 2020, Muñoz-Sabater et al, 2019, Benjamin et al, 2022, others), but lake temperature has not been a part of this surface data assimilation. In December 2020, the [two NOAA hourly updated weather models, the](#) 13-km Rapid Refresh (RAP) and 3-km High-Resolution Rapid Refresh (HRRR) implemented an interactive small-lake multi-layer 1-d lake model, the first NOAA weather models to do so. The lake [coverage](#) for the HRRR model is shown in Fig. 1 (RAP model lake coverage not shown). The HRRR and RAP weather models are coupled with the 10-layer Community Land Model (CLM) version 4.5 lake model, (Subin et al, 2012, Mallard et al, 2015), an option within the community Weather Research and Forecast model (WRF, Skamarock et al, 2019). The CLM lake model is a

Deleted: coverages

150 1-d thermal diffusion model allowing 2-way coupling with the atmosphere. Virtually no
 151 additional computational cost ($<0.1\%$) was added by use of the CLM lake model within
 152 the HRRR model. To initialize small-lake temperatures in the RAP and HRRR, all lake
 153 variables have been evolving (e.g., “lake cycling”) since summer 2018 depending on the
 154 cycled atmospheric conditions and the lake model physics as discussed in section 4.
 155 This cycling is similar to the land-surface cycling in HRRR and RAP as described by
 156 Benjamin et al (2022). The 1-d lake model cannot represent 3-d hydrodynamical
 157 processes in larger bodies of water. Thus, a second major improvement in 2020 with
 158 lake representation in the NOAA 3-km HRRR model occurred with the implementation
 159 of lagged data coupling with the 3-d hydrodynamic-ice model for the much larger
 160 Laurentian Great Lakes as described by Fujisaki-Manome et al (2020). **These new**
 161 **improved lake treatments are in the newer HRRR version 4 (HRRRv4) replacing the**
 162 **previous HRRRv3 (differences described in Dowell et al, 2022; hereafter D22).**



165
 166 Fig. 1. Small-lake areas for the 3-km HRRR domain using the MODIS 0.15” resolution
 167 data for land/water and lake information. Only small-lake areas treated in HRRR by the
 168 1-d CLM lake model are shown. A zoomed-in insert for HRRR small-lake coverage in
 169 the vicinity of the state of Wisconsin is shown in the lower left. Out of the 1,900,000
 170 grid points in this HRRR CONUS domain, 12,305 of them ($\sim 0.6\%$) are for small lakes
 171 (excluding the 5 Laurentian Great Lakes treated by separate coupling as described in
 172 text). Lakes circled in **black** were related to problem reports from US National Weather
 173 Service Forecast Offices on nearby deficient 2 m air temperature or dewpoint forecasts
 174 in NOAA hourly updated models as discussed in section 2.



Deleted:

Deleted: yellow

Here, we describe the design and results of a unique approach to inland-small-lake initialization by cycling with hourly updating of atmospheric conditions (clouds/radiation, near-surface temperature/moisture/winds). This lake initialization via cycling is an important component of earth-system coupled modeling for effective NWP, with goals to improve prediction of 2-m (air) temperature and moisture, cloud, boundary-layer conditions, and precipitation for situational awareness enabling short-range decision making (e.g., aviation, severe weather, hydrology, energy).

2 The Lake Initialization Problem

For the NOAA hourly updated mesoscale models, used frequently for short-range weather prediction, poor 2 m air temperature and/or dewpoint forecasts have been reported intermittently during 2004-2019 by the US National Weather Service (NWS) in the vicinity of inland lakes (Fig. 1). These hourly updated models included the Rapid Update Cycle (RUC, Benjamin et al, 2004) with horizontal grid spacing decreasing from 40-km to 20-km to 13-km (Benjamin et al, 2010), succeeded by the 13-km RAP, and 3-km HRRR (Benjamin et al, 2016, D22, James et al, 2022 (J22)). Many of these reported systematic deficiencies from the US NWS were for the 2.5-km NOAA Real-Time Mesoscale Analysis (RTMA, Pondeva et al. 2011), using 1-h forecasts from the 3-km HRRR as a background. The most common report was too-low 2 m air temperatures near inland lakes in late spring and summer. At times, spurious prediction of fog formation was also noted on or near small lakes due to too-cold lake temperatures and erroneous heat and moisture fluxes into the atmosphere.

Further investigation revealed the water temperatures for small lakes used in NOAA weather models were assigned via horizontal interpolation from larger, deeper bodies of water (with available AVHRR data) in the design for the NOAA real-time gridded SST analysis (RTG_SST_HR, Gemmill et al, 2007). An example of the analysis is shown in Fig. 2. Temperature for the larger, deeper water areas has a lesser and more lagged seasonal variation than the smaller, shallower lake areas due to their large heat storage capacity. Therefore, use of the NOAA SST fields for lake temperatures resulted in generally too-low values through spring and summer, and even into autumn. In situations with atmospheric cold outbreaks in the autumn, shallow lake temperatures quickly decrease (as reflected with lake cycling) and SST-based estimated lake temperatures were too high. This behavior was consistent with the HRRR and RTMA deficiencies noted by forecasters. In February 2020, NOAA changed from the RTG_SST_HR to a Near-Surface Sea Temperature (NSST, see NWS, 2020) for SSTs, but using the same horizontal interpolation method to estimate small-lake temperatures resulting in the same temperature biases for small lakes.

Deleted: Rapid Refresh (

Deleted:)

Deleted: High-Resolution Rapid Refresh (

Deleted: ,

Deleted: Dowell et al, 2022 (

Deleted:),

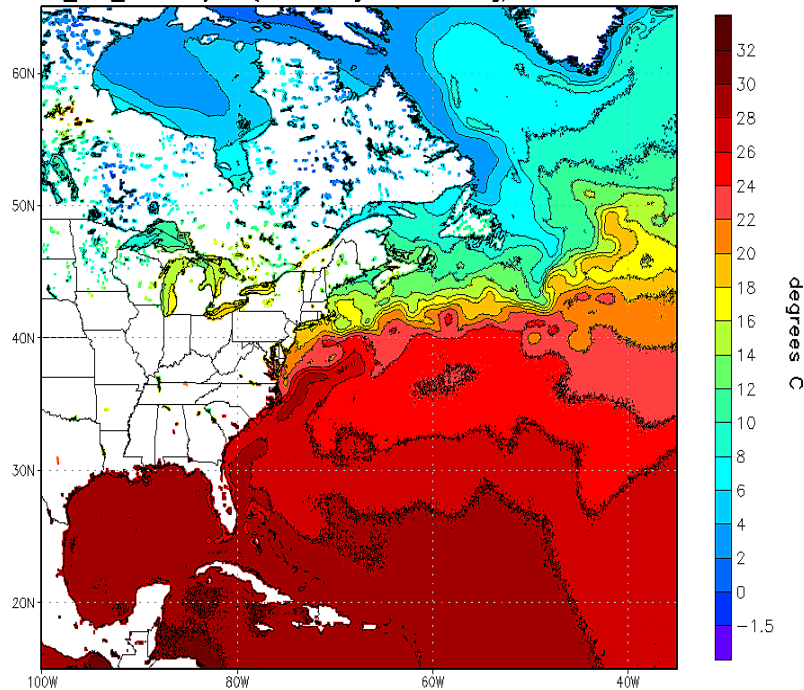
Deleted: erroneous

Deleted: resultant

Deleted: So

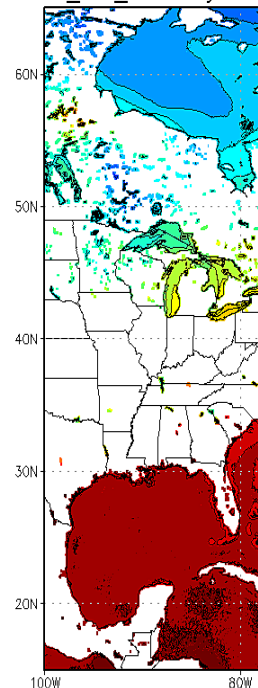
NOAA/NWS/NCEP/EMC Marine Modeling and Analysis Branch Oper H.R.

RTG_SST_HR Analysis (0.083 deg X 0.083 deg) for 09 Oct 2019



NOAA/NWS/NCEP/EMC Marine Modeling and Analysis Branch Oper H.R.

RTG_SST_HR Analysis (0.083 deg X 0.083 deg) for 09 Oct 2019



Deleted: 22:40:13 WED OCT 9 2019

Fig. 2. An example of small-lake temperatures spatially interpolated from deeper-water temperature data in the NOAA SST analysis (Gemmill et al, 2007). For 9 October 2019, provided by NOAA National Weather Service.

Hamill (2020), in a comparison benchmarking a statistical method for 2 m temperature (at 00 UTC), showed the same problem with large summer temperature biases from the HRRRv3 1-h forecasts in August 2018 especially in the vicinity of lakes (his Figs. 10, 11). His results are shown in Fig. 3, with three stations showing coldest biases (at 00 UTC) greater than 2 K (circled in red), all adjacent to lakes. In Fig. 3, these circled stations, from north to south, are KFGN (Flag Island on Lake of the Woods; > 3 K cold bias), KRRT - Warroad, MN (west of Lake of the Woods), and KVVU - Waskish, MN (east of Red Lake). The overall warm or cold biases are generally < 2 K, but these stations adjacent to lakes are outliers, consistent with introduction of cold-biased lake temperatures through the NSST.

Deleted: HRRR

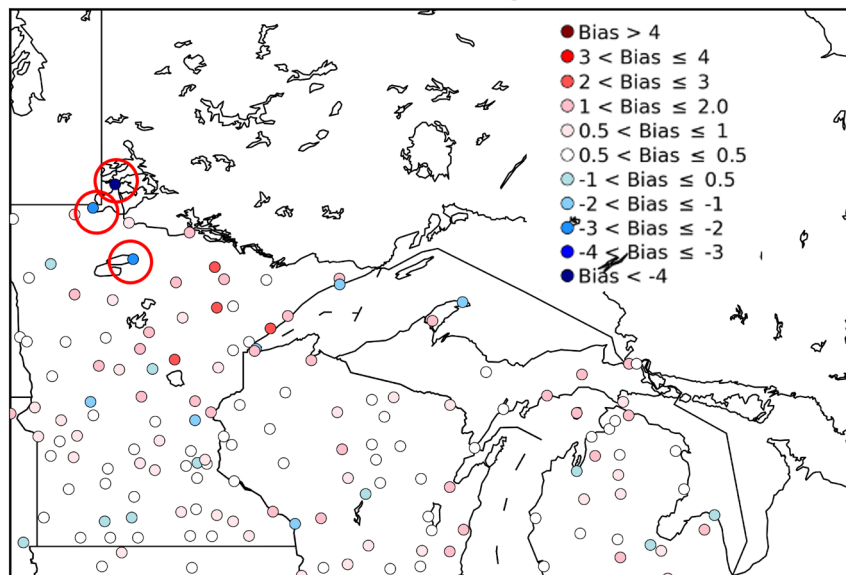


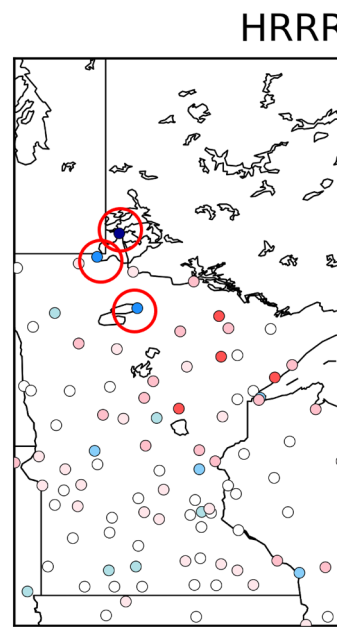
Figure 3. 2 m temperature biases for 1-h HRRR forecasts valid at 00 UTC in August 2018 (from HRRRv3, before introduction of lake cycling and using NSST estimates instead. HRRR versions and dates are listed in D22.). Stations with low bias < -2 K are circled in red. (Credit and thanks to Thomas Hamill, providing a regional version of his Fig. 10b in Hamill, 2020).

With its 3 km grid spacing, the HRRR model can resolve many inland lakes (Fig. 1). Specification of surface temperatures for these small lakes using the horizontal interpolation from the NOAA SST fields was problematic being determined by interpolation from large lake and ocean temperatures.

In summary, errors in specified lake temperatures (as well as ice cover and concentration) due to spatial interpolation from oceans and larger lakes can lead to degraded atmospheric predictions in the vicinity of lakes. For small lakes, poor short-range 2 m temperature (T) and 2 m dew point temperature (T_d) forecasts were noted in vicinity of lakes, especially from spring through summer and into autumn. Specifically, fluxes from lakes were often poorly estimated due to inaccurate lake temperature fields.

3 Lake model for coupling with NOAA regional atmospheric models

To complement the now-commonplace (in NWP models) coupling with land-surface models (LSMs) to improve fluxes into the atmosphere, a multi-level 1-d lake model was



Deleted:

Deleted: ¶

Deleted: Similar to

273 implemented within the operational 3-km **HRRRv4** and 13-km RAP weather models in
274 December 2020, an extension to atmosphere-surface coupling. An effective lake
275 initialization is a necessary complement for the lake model coupling, as described in
276 section 4. Different earth-system coupling processes represented in the HRRR and
277 RAP models are described in Table 1, including land, snow, ice, and smoke. The
278 Community Land Model (CLM) lake model (same in versions 4.5 and 5.0) was added
279 for smaller lakes as an option in the WRF model version 3.6 (Mallard et al, 2015). The
280 CLM lake model is described in more detail below with its configuration for the NOAA
281 **HRRRv4** and RAP weather models. A detailed description of the physical processes
282 (cloud microphysics, turbulent exchange, land-surface, etc.) in the HRRR and RAP
283 models are described by D22 and Benjamin et al (2016).

Deleted: HRRR

Deleted: HRRR

Component	Prognostic variables	Layers (below surface except for smoke)	Year introduced for experimental cycling	Year intro for NCEP	Data assimilation	Other information, references
Soil	Temp, moisture	9	1996 (6 levels until 2012)	1998 (6 levels until 2014)	Cycling, atmos-to-soil coupled DA	Moderately coupled DA (Benjamin et al 2022)
Snow	Water equiv, snow depth, temp	2	1997	1998	Cycling, atmos-to-snow DA for temp, trim/build from sat for cover	Moderately coupled DA . Subgrid fraction intro 2020
Ice	Temp	9	2010 (6 levels until 2012)	2012 (6 levels until 2014)	Cycling, atmos-to-surface coupled DA	Subgrid fraction intro 2018
Smoke	Smoke mixing ratio	50 atmos layers	2016	2020	Cycling, fire rad power from sat	No direct DA, only cycling
Small lakes	Temp, ice fraction, mixing	10	2018	2020	Cycling	No direct DA, only cycling
Large lakes (Great Lakes)	Temp, ice fraction, mixing	FVCOM levels	2018	2020	Independent	FVCOM driven by HRRR wind, rad, temp, 6h lag (Fujisaki-Manome et al 2020)

Table 1. Earth-system coupling added to NOAA regional models (HRRR, RAP, RUC (pre-2012)).

Deleted:))

An additional improvement in lake-atmosphere coupling in NOAA weather models for large lakes (>15,000 km²) was recently introduced, a coupling between the NOAA HRRR model using predicted lake temperatures and ice concentration fields from the NOAA GLERL/NOS 3-dimensional hydrodynamic-ice model run in real time over the Laurentian Great Lakes, as described by Fujisaki-Manome et al (2020). This hydrodynamic-ice model is based on the Finite Volume Community Ocean Model (FVCOM, Chen et al., 2006, 2013) coupled with the unstructured grid version of Los Alamos Sea Ice Model (CICE; Gao et al., 2011) and is applied to the NOAA Great Lakes Operational Forecast System (GLOFS, Anderson et al., 2018). This time-lagged data coupling (alternate applications of HRRR atmospheric forcing and FVCOM-CICE lake forcing about 6-12 h in advance) was incorporated to improve lake-effect snow (LES) predictions in winter but has also been found to improve near-lake atmospheric predictions year-round especially for upwelling events in the warm season. The use of FVCOM-CICE to specify lake temperatures addresses previous errors in SST from relatively fast changes in lake temperatures due to cold air outbreaks or upwelling

events. These changes sometimes escape AVHRR-derived SST detection due to multi-day cloud obscuration.

Small lake size (grid points)	# Lakes	% of # of small lakes	% of small lake surface coverage	Avg depth (m)	Surface area of lakes (km ²)	Volume of lakes (km ³)
1 grid point (3kmx3km)	917	49%	7%	13	8,812	115
2 (~20 km ²)	323	17%	5%	12	6,208	76
3	155	8%	4%	11	4,468	49
4-5	157	8%	6%	14	6,746	97
6-10 (~100 km ²)	155	8%	10%	14	11,570	162
11-100 (~1000 km ²)	141	7%	30%	21	35,518	769
>100	16	<1%	38%	14	44,926	614
All	1864	100%	100%		118,248	1,882

Table 2. Characteristics of small lakes (not including the five Laurentian Great Lakes) resolved in the 3-km ~~HRRRv4~~ CONUS domain over the lower 48 United States and adjacent areas of Canada and Mexico. Grid points were assigned as having a lake land use for points with at least 50% lake representation from the higher-resolution 15" MODIS land-use data.

Laurentian Great Lakes	Surface area of lakes (km ²)	Volume of lakes (km ³)
Superior	82,100	12,000
Michigan	57,800	4,920
Huron	59,600	3,540
Erie	25,670	484
Ontario	19,010	1,640

Table 3. Characteristics of the five Laurentian Great Lakes (surface area, volume) (Hunter et al 2015).

Deleted: HRRR

3.1 CLM lake model applied to HRRR for smaller inland lakes

Subin et al (2012) describe the 1-d CLM lake model as applied within the Community Earth System Model (CESM) as a component of the overall CESM CLM (Lawrence et al 2019). Gu et al (2015) describe the introduction of the CLM lake model into the WRF model and initial experiments using its 1-d solution for both Lakes Superior (average depth of 147 m) and Erie (average depth of 19 m). The CLM lake model divides the vertical lake profile into 10 layers driven by wind-driven eddies. The atmospheric inputs into the model are temperature, water vapor, horizontal wind components from the lowest atmospheric level and short-wave and longwave radiative fluxes (from the HRRR model in this application). The CLM lake model then provides latent heat and sensible heat fluxes back to the HRRR. The CLM lake model is called every 20 s within the HRRR model. The CLM lake model was configured with the top layer fixed to a 10-cm thickness (Gu et al 2015) and with the rest of the lake depth divided evenly into the other 9 layers. Energy transfer (heat and kinetic energy) occurs between lake layers via eddy and molecular diffusion as a function of the vertical temperature gradient. The version of the CLM lake model used for ~~HRRRv4~~ and RAP was introduced with CLM version 4.5 and continues without change in CLM version 5 (Lawrence et al, 2019). The CLM lake model also uses a 10-layer soil model beneath the lake, a multi-layer ice formation model and up to 5-layer snow-on-ice model (Gu et al, 2015). ~~Again, testing~~ of the CLM lake model by the authors within WRF showed computational efficiency of the model with no change of even 0.1% in run time with the HRRR and RAP applications. Multiple layers in lake models better represent vertical mixing processes in the lake. By intention, the CLM lake model was only applied for HRRR and RAP model to smaller lakes, since NOAA began at the same time to provide temperature and ice cover through GLOFS for the Laurentian Great Lakes through the 3-d hydrodynamic-ice model (Fujisaki-Manome et al, 2020, Anderson et al, 2018).

Deleted: HRRR

Deleted: Testing

3.2 Lake area mask

Grid points were assigned as lake points when the fraction of lake coverage in the grid cell (derived from yet finer 15" MODIS data) exceeds 50% and when HRRR gridpoint elevation > 5 m above sea level (ASL, to distinguish from ocean) and is disconnected from ocean areas with the 3-km land-water mask. The lake water mask is therefore binary, set to either 1 or 0. This binary approach at 3 km seemed capable of capturing the effect of lakes on regional heat and moisture fluxes. The alternative subgrid lake fraction approach was used by ECMWF with their 9-km model (Choulga et al, 2019).

An overview of the lake number, areal coverage, and integrated volume for the 3-km ~~HRRRv4~~ model are depicted in Table 2. The HRRR CONUS domain (Fig. 1) is able to represent 1864 separate lakes occupying 0.6% of the entire domain. These water bodies represented in HRRR as "lakes" include reservoirs and larger rivers, and about half of the 1864 lakes are single-gridpoint lakes. The sixteen largest lakes in the HRRR CONUS domain have surface area greater than 1,000 km², nine in Canada and two on

Deleted: HRRR

the US-Canada border (Lake of the Woods and Lake St. Clair). In contrast, the five Laurentian Great Lakes (Table 3) range in size from 82,000 km² (Superior) to 19,000 km² (Ontario), and therefore, their representation in the coupled HRRR system (Table 1) is handled with 3-d hydrodynamic-ice models (Fujisaki-Manome et al, 2020).

The lake area mask for the 3-km HRRRv4 used an algorithm for identifying an ocean area mask for all areas with contiguous water areas and leaving other areas also below 5 m ASL as near-ocean lagoon regions treated as lakes with the CLM 1-d lake model. These lagoon areas separated from ocean by barrier islands in the HRRR representation (Fig. 1) include the Intracoastal Waterway in Texas largely separated from the Gulf of Mexico by Padre Island, Indian River in Florida largely separated from the Atlantic Ocean by Merritt Island, and Lake Pontchartrain in Louisiana. This ocean-contiguity technique is similar to the flood-filling technique used by ECMWF (Choulga et al, 2019).

3.3. Lake depths

Lake depths for the HRRRv4-WRF-CLM lake configuration (Fig. 4) are assigned from a global dataset provided by Kourzeneva et al (2012b, hereafter K12). For some smaller lakes identified using the 15" MODIS land-water mask not found in K12, a 50 m depth was assumed (too deep, will be reduced in future). K12 identified uncertainties in their own database including estimates of lake depth and errors in coastlines. More recently, ECMWF applied a 10 m depth as a default depth for these small lakes (Choulga et al, 2019). For many lakes in the K12 database, a single value for maximum lake depth had been applied to all lake points, which results in excessive lake water volume and too cold temperatures as discussed in section 5. However, the K12 database still allows overall differentiation between shallow and deep lakes.

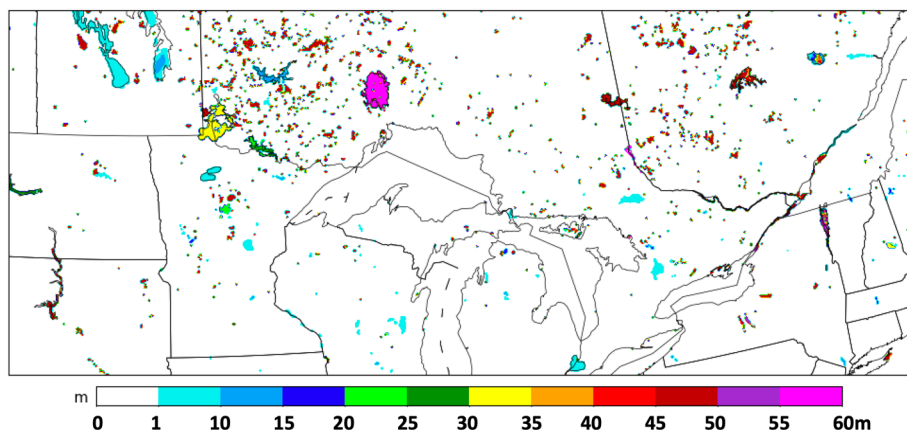


Figure 4. Lake depth for small lakes in a subset of the HRRR domain.

Deleted: HRRR

Deleted: 25

Deleted: The majority of the small lakes in the northern US and southern Canada are assigned as shallow, at 5 m depth, but a few are assigned a depth as 30 m or deeper (Fig. 4).

Deleted:

Deleted: with red for lakes 30 m or deeper

405

406 3.4 Turbidity

407

408 A single value for turbidity to describe absorption of downward short-wave radiation is
409 used in CLM, allowing for a moderate amount of suspended sedimentation. Subin et al
410 (2012) describe other options for variations in radiative transfer in lake bodies to capture
411 degrees of eutrophication, but these are not used here.

412

413 3.5 Salinity

414

415 The CLM lake model is configured for fresh water. The authors manually modified the
416 freezing temperature to account for non-zero salinity (Railsback, 2006) from 0°C to -5°C
417 for Mono Lake in California and Great Salt Lake (GSL) in Utah to capture the effect of
418 salinity. Other areas of water impoundment from coastal lagoons in the 3-km HRRR
419 lake representation (Fig. 1) also have, in reality, non-zero salinity (e.g., along coasts of
420 Gulf of Mexico and Atlantic Ocean) but this is not applied in HRRR/RAP. Moreover, no
421 change in freezing temperature is necessary for these areas anyway.

422

423 3.6 Elevation

424

425 The elevation value (above sea level) assigned to each lake grid point is the same
426 assigned to that from the atmospheric model, which may be different from reality, but at
427 least consistent with the atmospheric conditions. As mentioned earlier, the minimum
428 elevation above sea level of a grid point to be assigned as a lake is 5 m; other water
429 grid points are assumed to be ocean.

430

431 3.7 Special situations for CLM lake model application

432

433 The algorithm for the turbulent heat flux calculation in the CLM-lake model was mainly
434 based on Zenget al. (1998), except that roughness length scales for temperature and
435 humidity are the same as roughness length scale for momentum for its WRF-lake
436 application, while they are updated dynamically in CLM 4.5. Charusombat et al (2018)
437 showed that the same roughness length scales for temperature and salinity as that for
438 momentum could result in overestimated surface sensible and latent heat fluxes in
439 autumn and winter. Therefore, a revision to the CLMv4.5 lake model was introduced for
440 modified roughness lengths over water using modified formulations of the Coupled
441 Ocean-Atmosphere Response Experiment (COARE) algorithm as described by
442 Charusombat et al (2018) to improve surface sensible and latent heat fluxes.

443

444 For GSL with a very high value of salinity (270 ppt north of ~41.22°N with freezing point
445 of 249 K and 150 ppt south of ~41.22°N with freezing point at 263 K), a change of
446 freezing temperature to -5°C appeared to be not sufficient to keep the lake ice-free
447 during the cold outbreaks in winter in this high-elevation area. GSL is unusual in various
448 aspects – it is hypersaline (far more saline than the ocean), the largest terminal lake

Deleted: ¶

(without outflow) in the Western Hemisphere (Belovsky et al, 2011), shallow (mean depth of 5 m) and subject to very strong eutrophication (Belovsky et al, 2011). According to GSL climatology the lake stays ice-free all winter, and its temperature goes slightly below freezing only for a very short period in January and February. Thus, we presume that the CLM lake model needs to allow turbidity variation (see section 3.4). A solution to this representation problem was use of a bi-weekly climatology over each 1-year period to bound the cycled GSL temperature at initial forecast time not to deviate more than $\pm 3^{\circ}\text{C}$ from the climatological value interpolated to the current day of year. Also, using special code, GSL was forced stay ice-free for the whole year as observed.

3.8 Time step

The CLM lake model within the HRRR/RAP weather models was run with the same time step as for other physical processes in the HRRR model (20 s) and the RAP model (60 s). Again, even with this relatively high frequency for calling the CLM lake model, the computational expense was extremely small, less than 0.1% of overall HRRR run time.

4 Initialization for small lake temps by cycling with ongoing atmospheric predictions – a strategy

The central strategy described in this paper is to use accurate, ongoing atmospheric forcing with a computationally inexpensive 1-d lake model to obtain an equilibrium state of a lake temperature profile. This technique responds appropriately to strong changes in atmospheric forcing (e.g., cold air outbreak or excessive heat events). With the NOAA HRRR and RAP atmospheric models performing hourly data assimilation of a broad set of hourly observations, accurate atmospheric forcing is available.

The RAP and HRRR hourly data assimilation cycles include these aspects, all of which are important for cycling initialization of inland lakes. First, cloud assimilation (from satellite and ceilometer data) to ensure accurate shortwave and longwave radiation fields (Benjamin et al 2021). Second, radar reflectivity data are assimilated as part of a 3-km ensemble data assimilation system to ensure accurate short-range precipitation (Weygandt et al, 2022, D22, J22, Benjamin et al, 2016). Finally, 2 m air temperature and moisture and 10 m wind observations are effectively assimilated (i.e., producing more accurate predictions) including representation through the boundary layer using pseudo-innovations (James and Benjamin, 2017, meaning estimated observation-background forecast differences but not actual). Other information on the HRRR/RAP data assimilation is provided by Benjamin et al (2016) and D22.

The cycling of the 10-level CLM lake model within the ~~then~~-experimental HRRRv4 started on 24 August 2018. After 10 days of cycling (Fig. 4), differences in lake temperatures between HRRRv4 and the operational HRRRv3 using interpolated NSST

data were evident of 5-15°F (3-12°C or 276-285 K), showing that the adjustment with realistic atmospheric conditions and use of the CLM lake model with roughly accurate lake depth data was very effective.

Consequences (to right) from strategy for lake initialization (below)	Coupling lake and atmosphere within initialization	Lake temps in spring-summer	Lake temps in fall
SST interpolation to small lakes	None	Much too cold, especially for shallow lakes	Still generally too cold but intermittently too warm after cold-air outbreaks.
Lake annual variation forced by reanalysis atmospheric data – 1-way cycling from atmospheric forcing	1-way	More accurate. No weather regime variation in a given year	More accurate. Will not capture variation from weather regimes in a given year.
Daily updating with satellite data	None	More accurate but cannot keep up with changes during cloudy periods.	More accurate but cannot keep up with changes during cloudy periods.
2-way coupled cycling	2-way	More accurate including response to specific yearly/seasonal anomalies.	More accurate including yearly/seasonal anomalies

Table 4. Expected seasonal lake-atmosphere temperature consequences from different lake initialization strategies

Possible approaches for initializing lake temperatures are summarized in Table 4. The simplest option is via larger-scale water temperature data (SST data) with horizontal interpolation to smaller water areas including inland lakes and reservoirs; this was the previous strategy for the HRRRv3 and older RAP models before introduction of cycling using the CLM lake model. An alternate strategy is to run lake models over a multi-year period forced by reanalysis atmospheric data (ERA-Interim) as described by Balsamo et al (2012), Dutra et al (2010), and Balsamo (2013) for the ECMWF to obtain a yearly varying climatology of lake temperature for all lakes represented. This method will capture the mean annual variation of lake temperatures. However, due to multi-year averaging, it cannot represent anomalous conditions in a given year (sustained heat or sustained cold conditions), which can modify temperatures especially for shallow lakes by several K within 1-2 weeks. Use of daily updating from satellite data can be effective (e.g., MetOffice – Fiedler et al, 2014) under clear-sky conditions. Full cycling of the lake model within an ongoing coupled weather model, the strategy described in this paper, can represent the lingering effects of anomalously warm or cold weather upon lake temperatures and the resultant fluxes.

Deleted: ¶

Deleted: HRRR

The 2-way coupled cycling (Table 4) used now in the HRRR and RAP models benefit via hourly data assimilation using latest hourly observations both for the atmosphere (D22) and land-surface snow conditions (Benjamin et al 2021). In the 3-km HRRR model, the 3-d state of the atmosphere, land surface, and inland lake conditions are advanced on 20-second time steps using the HRRR-specific configuration (described in D22) of the WRF model (Powers et al, 2017; Mallard et al, 2015). As atmospheric conditions change every 20 s (including temperature, moisture, wind, and radiation), the exchange of heat, moisture, and momentum between inland lake points and the atmosphere also vary. Lake temperature is not modified in the hourly data assimilation step, but the ongoing exchange recalculated every 20 s forces an evolution of lake conditions to values consistent with atmospheric conditions. ECMWF applies a similar ongoing cycling for lake prognostic variables (ECMWF, 2020) for lake initialization.

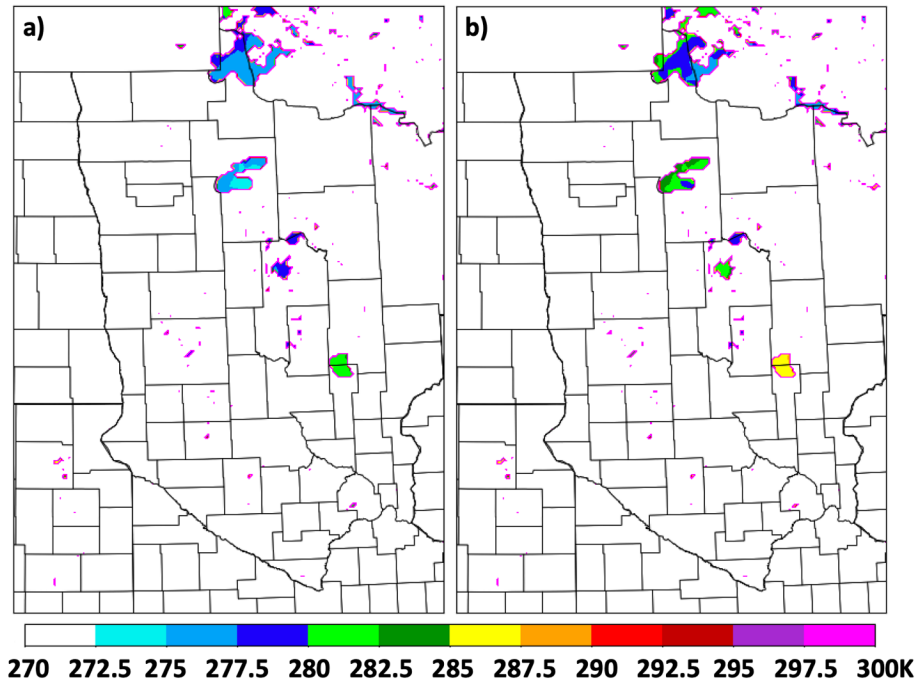


Figure 5. Lake surface temperatures from 18-h forecasts valid at 1500 UTC 3 September 2018 for a) operational HRRRv3 using NSST for lake temperatures, and b) then-experimental HRRRv4 with CLM lake model and cycling.

Deleted: <object> ... [2]

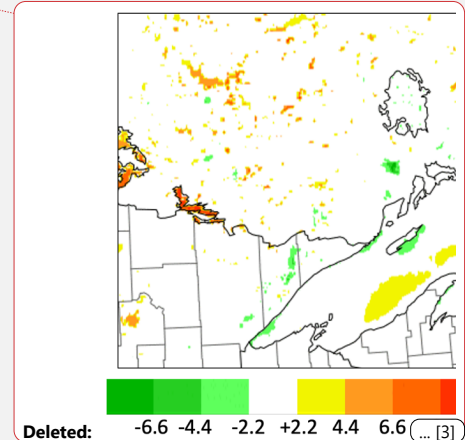
Deleted: Skin temperature (K) including lake
Deleted: . From
Deleted: 15

A similar challenge is initialization of lake ice cover. Similar to the treatment for lake temperature, cycling of a multi-level lake model (like the CLM lake model) can provide an alternative, adaptive-in-time method for lake-ice initialization. NOAA has used in the HRRR and RAP the daily IMS ice cover product¹ (US National Ice Center, 2008) for binary (non-fractional) lake ice cover. The IMS ice cover is used for oceans and large lakes (e.g., for RAP for Great Slave Lake and Great Bear Lake in northern Canada). For small lakes below the resolution of the IMS ice map, lakes stayed open for the winter. Starting with HRRRv4 and RAPv5, ice concentration from the NOAA global model is used for oceans, FVCOM ice fraction is used for the Great Lakes, and ice fraction from the CLM lake model for small lakes.

5 Results

In this section, we describe comparisons of lake surface temperature evolution between the CLM implementation described here and the lake specification through interpolation from the NSST dataset (Fig. 2) at lakes in the United States and southern Canada.

Comparisons during 2018–2019 were drawn from real-time simulations from the then-operational HRRRv3 (using interpolated SST) and the ~~then~~-experimental HRRRv4 (using CLM). More recent comparisons were made for March–November 2021 between the operational HRRRv4 (using CLM) and interpolated NSST values (as used in 2019–2020 for HRRRv3). In addition, the CLM and NSST values were compared to in situ observations where available and also to satellite-based estimates defined below.



¹ <https://usicecenter.gov/Products/ImsHome>

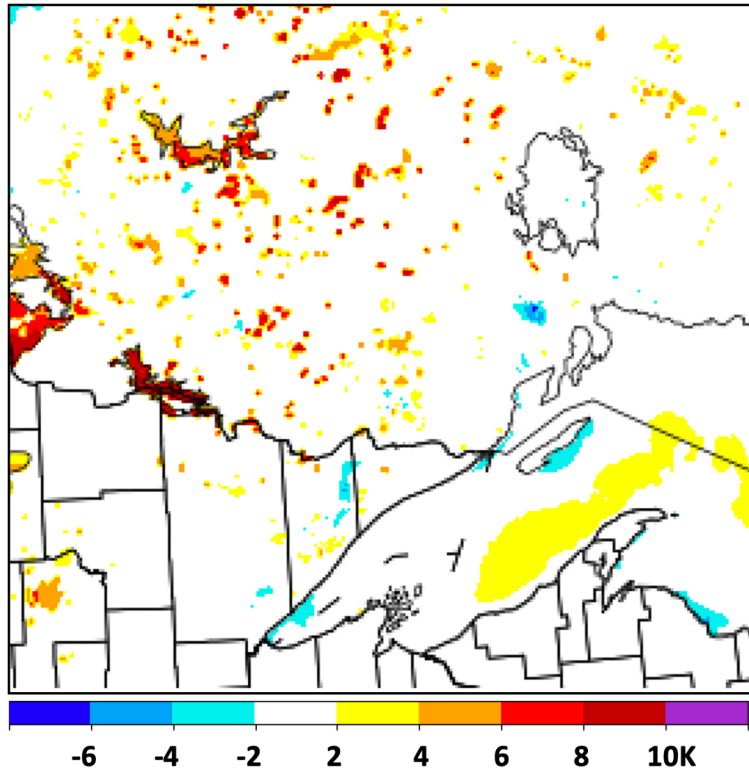


Figure 6. Difference (K) in lake surface temperatures between versions of HRRR model using cycled lake-model values (HRRRv4) and using interpolated NSST data (HRRRv3). Valid 1300 UTC 13 October 2019, and also includes differences from use of FVCOM lake model in HRRRv4 (Fujisaki-Manome et al, 2020).

5.1 Cases from 2018 – 2019

Introduction of the CLM lake model forced by ongoing HRRRv4 atmospheric conditions (i.e., cycling) allowed, within only 10 days, an increase in lake temperatures for Red Lake and Lake of the Woods (both in Minnesota) from 3 K to over 10 K (Fig. 5) in September 2018. A comparison in skin temperature for a year later (October 2019) between versions of the HRRR model (HRRRv4 with lake cycling vs. HRRRv3) including differences from with and without lake cycling is shown in Fig. 6. Higher temperatures were evident for the Minnesota/Ontario lakes from cycling (vs. NSST interpolation). HRRRv4 also included coupling with the 3-d FVCOM lake model for

Formatted: Font: Italic

Formatted: Line spacing: Multiple 1.15 li

Deleted: skin temperature (including

Deleted:)

Deleted: or HRRRX

Deleted:

Deleted: or HRRR-NCEP

the Laurentian Great Lakes, showing areas of upwelling with associated cooler water over Lake Superior in Fig. 6 from predominant westerly to southwesterly near-surface wind at this time.

Lake number	Lake name	State/province, country	HRRR l point	HRRR j point	Area (km ²)	Depth used (m)	Ice free?
1	Simcoe	ON, CA	1378	799		6	N
2	St. Clair	ON/MI, CA/US	1302	709	1240	6	N
3	Champlain	VT/NY, US	1534	835		77	N
4	Sebago	ME, US	1610	833		33	N
5	Okefenokee	FL, US	1459	145	1510	3	Yes
6	Pontchartrain	LA, US	1136	224	2180	10	Yes
7	Intracoastal Waterway (near Corpus Christi, TX)	TX, US	905	128	3300	10	Yes
8	Salton Sea	CA, US	337	387		9	Yes
9	Tahoe	NV/CA, US	259	628		313	N
10	Great Salt	UT, US	486	653	3050	3	Yes
11	Utah	UT, US	496	622		3	N
12	Bear	ID/UT, US	518	684		29	N
13	Sakakawea	ND, US	790	868		27	N
14	Winnebago	WI, US	1143	742		7	N
15	Lower Red	MN, US	961	880		5	N
16	Lake of the Woods	MB/MN, CA/US	965	919	3030	32	N
17	Manitoba	MB, CA	879	972	3240	5	N
18	Winnipeg	MB, CA	916	977	13270	8	N
19	Nipigon	ON, CA	956	956	5410	55	N

Table 5. Lakes for comparison of lake surface temperatures between HRRRv4/CLM, NASA SPoRT, NSST, and in situ observations as shown in Figs. 7 and 8. Area is shown for lakes >1000 km². Lake depths are constant within each lake except for lakes 2, 3, and 18. See Fig. 4 for example map of lake depth used in HRRR. Specific HRRR i/j 3-km grid points (indicated in table) were selected from HRRR data for each lake.

Deleted: HRRR

602
603

Name of Lake	No. from Tab. 5	Source of Observation	Depth of Sensor (m)	URL
Lake St. Clair	2	ECCC	6	https://www.ndbc.noaa.gov/station_page.php?station=45147
Lake Champlain - Schuyler Reef	3	GLERL	0.45	https://www.ndbc.noaa.gov/station_page.php?station=45195
Sebago Lake @ Lower	4	Portland Water District Buoy	Est 1	https://www.pwd.org/sebago-lake-monitoring-buoy
Lake Pontchartrain @ New Canal Station	6	NOAA/ National Ocean Service	0.6	https://www.ndbc.noaa.gov/station_page.php?station=nwcl1
Intracoastal Waterway @ Baffin Bay near Padre Island	7	Texas Coastal Ocean Observing Network	unknown	https://www.ndbc.noaa.gov/station_page.php?station=babt2
Lake Tahoe	9	NASA/JPL	0.5	https://laketahoe.jpl.nasa.gov/get_imp_weather
Utah Lake @ Provo Marina	11	Utah DWQ Water Quality Network	unknown	https://wqdatalive.com/public/669
Bear Lake	12	Utah DNR State Parks	unknown	https://stateparks.utah.gov/parks/bear-lake/current-conditions/
Lake Sakakawea @ Missouri River near Williston, ND	13	USGS	unknown	https://waterdata.usgs.gov/monitoring-location/06330000/#parameterCode=00065&period=P7D

604
605
606

Table 6. Sources of available in situ data among 19 lakes in Table 5.

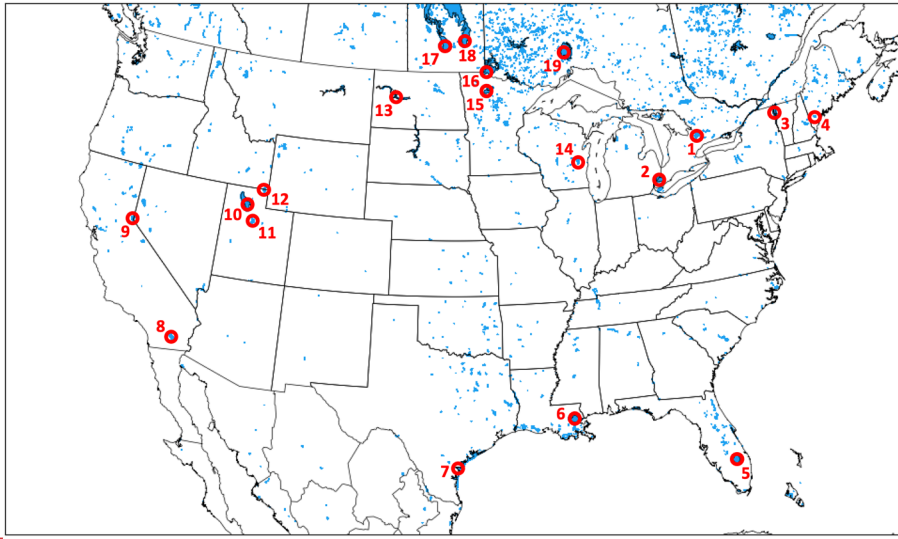
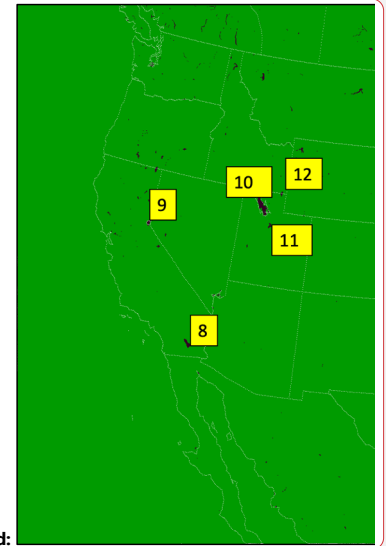


Figure 7. Locations of 19 lakes (see Table 5) used for the lake surface temperature intercomparison in this paper in Fig. 8. These lakes are shown as mapped onto the 3-km CONUS HRRR model domain.

5.2 Comparisons of different lake temperature estimates for 19 lakes from lower 48 US and southern Canada during 2021.

During a period from March to November 2021, a comparison was made of lake surface temperatures between the cycled HRRRv4-CLM values and those from three other estimates from NASA, NOAA, and in situ observations. A geographically diverse set of 19 lakes over the lower 48 United States and southern Canada was selected for these comparisons as listed in Table 5 and shown in Fig. 7. Lakes selected included near-ocean lagoon areas separated from ocean areas by coastal land as resolved by the 3-km land-water mask as discussed in section 3.2. The water areas also included a reservoir (Lake Sakakawea). Some of these lakes are dimictic or polymictic (with ice cover part of each year, Lewis 1983) but five of them do not experience any ice cover (Table 5), and lakes 5, 6, 7, and 8 are monomictic. The CLM lake model was cycled for all these lakes in the 3-km HRRRv4 model. The 19 lakes included seven lakes with a surface area greater than 1,000 km². The March–November evaluation period include the spring–summer warming period and the cooling period in autumn. Data points were obtained monthly for March–August and weekly for September–November.



Deleted:

Deleted: HRRR

Deleted: HRRR

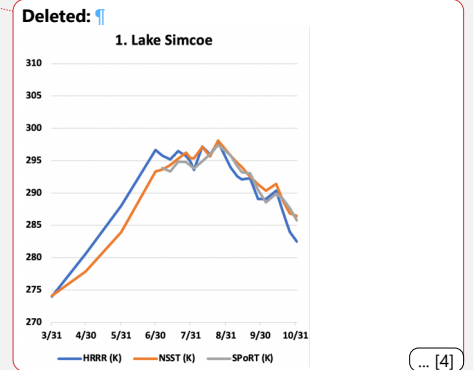
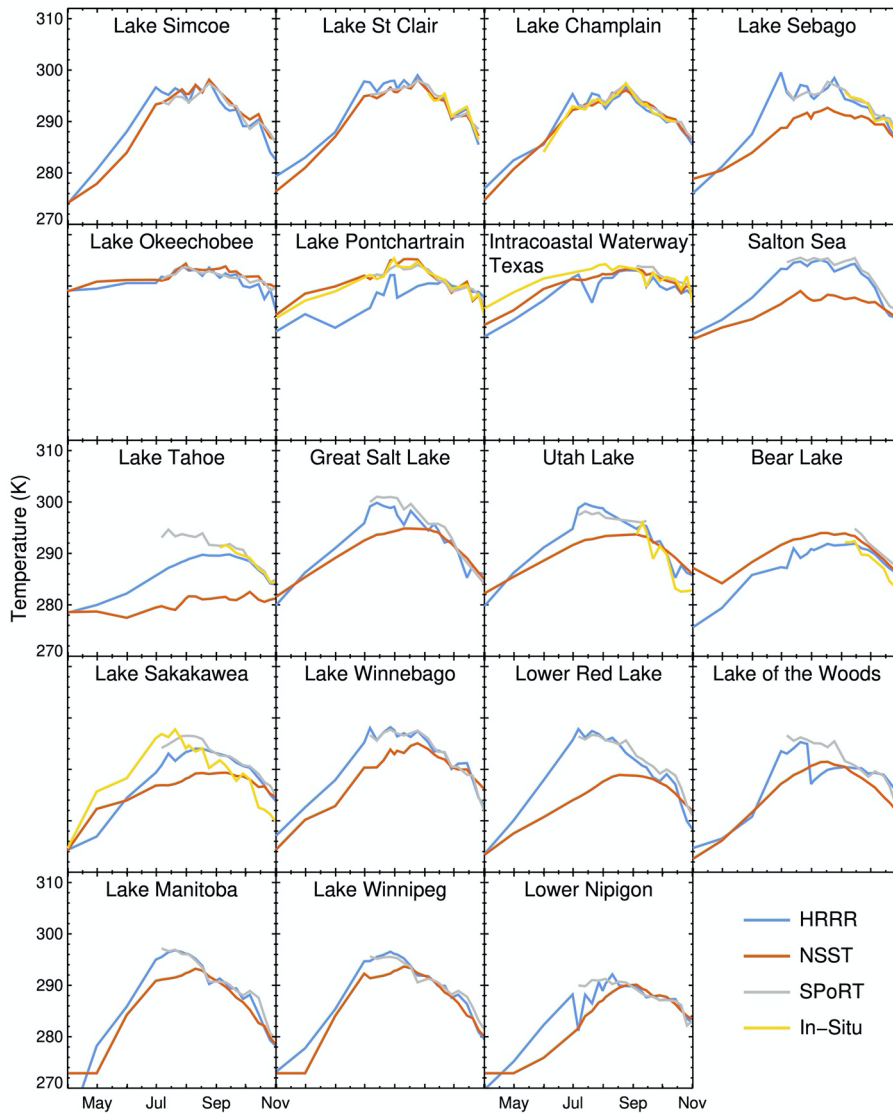


Figure 8. Lake surface temperatures in 2021 (April-October) from the 19 selected lakes (Table 5, Fig. 7) from HRRR-CLM-cycled, NSST, SPoRT, and in situ data.

Deleted: (blue),
 Deleted: (red),
 Deleted: (gray),
 Deleted: (orange).

647
648

649 The ~~HRRRv4~~-CLM values for these 19 lakes were compared with first, an estimate from
650 NASA SPoRT (Short-Term Prediction Research and Transition) real-time surface water
651 temperature composite including time-weighted MODIS and VIIRS data for inland lakes
652 (NASA, 2021, Kelley et al, 2021). The SPoRT estimates are similar to the satellite-
653 based lake temperature estimates from the Met Office (Fiedler et al 2014). The SPoRT
654 composite is valid from the surface to 2 m depth and is averaged over a 7-day period to
655 mitigate for cloud cover on a given day. A second lake temperature estimate is that from
656 NSST, as discussed earlier. Third, in situ surface water temperature observations were
657 available from observing platforms in nine of the 19 lakes (Table 6). The platforms are
658 operated by Federal, state, and local government agencies and a regional ocean
659 observing system. The depths of the water temperature observations were only
660 available at four of the nine platforms. At these four sites, the depth ranged from 0.45 to
661 0.9 m.

Deleted: HRRR

662

663 In general, the ~~HRRRv4~~-CLM-cycled lake ~~surface~~ temperatures showed the anticipated
664 difference from NSST values with quicker summer warming from HRRR-CLM cycling for
665 all lakes except the southern 3 lakes (5, 6, 7 in Table 5, with Lakes 6 and 7 essentially
666 lagoons in close proximity to the ocean) and Bear Lake in UT/ID (Lake 12, 39 m depth).
667 The NSST estimates were colder for spring through summer than HRRR values for 15
668 of the 19 lakes, a consequence from the NSST estimate via horizontal interpolation from
669 deeper bodies of water.

Deleted: HRRR

670

671 For the nine lakes with in situ observations (Table 6), the HRRR-CLM-cycled lake
672 temperatures are generally able to better capture weekly variability in summer and
673 autumn months, associated with windy periods increasing mixing or relatively warm and
674 cool weather periods or varying amounts of cloud cover. This can be seen, for
675 example, at Utah Lake and the Intracoastal Waterway west of Padre Island in Texas
676 (note cooling from passage of Hurricane Nicholas in mid-September). The most
677 dramatic improvement of HRRR-CLM over NSST lake temperatures is seen at Lake
678 Tahoe and lakes 14-19 in the northern region, with NSST estimates 5-10 K too cool. At
679 two of the lakes with in situ observations, the Intracoastal Waterway (linked to the
680 ocean) and Lake Pontchartrain, both lagoons linked to the ocean, NSST estimates are
681 generally closer than HRRR-CLM to the observations.

682

683 HRRR-CLM lake ~~surface~~ temperatures matched in situ observations well for the
684 northern lakes, usually within 1-2 K. In contrast, the lake temperature values from
685 SPoRT were generally warmer than HRRR or in situ observations in the autumn period.
686 The SPoRT observations showed a strong confirmation of HRRR-CLM-cycled lake
687 temperatures for lakes in the western US (Lakes 8-13) and most lakes in the northern
688 areas (Lakes 4, 14-19). Finally, the HRRR-CLM-cycled lake temperatures during this
689 period often varied strongly from the NSST estimates, with differences of up to 5-10 K
690 (largest difference with Red Lake, Lake 15). The effect of lake depth was evident with

a faster transition to fully mixed lakes for shallow lakes (e.g., 5 m depth for Red Lake in MN, Lake 15 in Table 5) but subject to more temporal and horizontal variation for deeper lakes. Fig. 9 showed a strong intralake variation of 7 K across Lake of the Woods (32 m depth) in the HRRR-CLM estimate in contrast with very little variation (< 1 K) across Red Lake. Due to a lack of high-resolution observations of lake surface temperatures, it is difficult to determine which intralake variations are more realistic. However, we think some of these intralake contrasts from HRRR-CLM may be exaggerated from actual values, possibly requiring a future introduction of a small temperature exchange rate (diffusion) between adjacent lake columns. Differences in skin temperature (e.g., SPoRT) and bulk temperature (e.g., in situ) for lakes have been noted (e.g., Wilson et al, 2013) of up to 0.5 K, but the HRRR vs. NSST differences in this study are generally much larger than this magnitude.

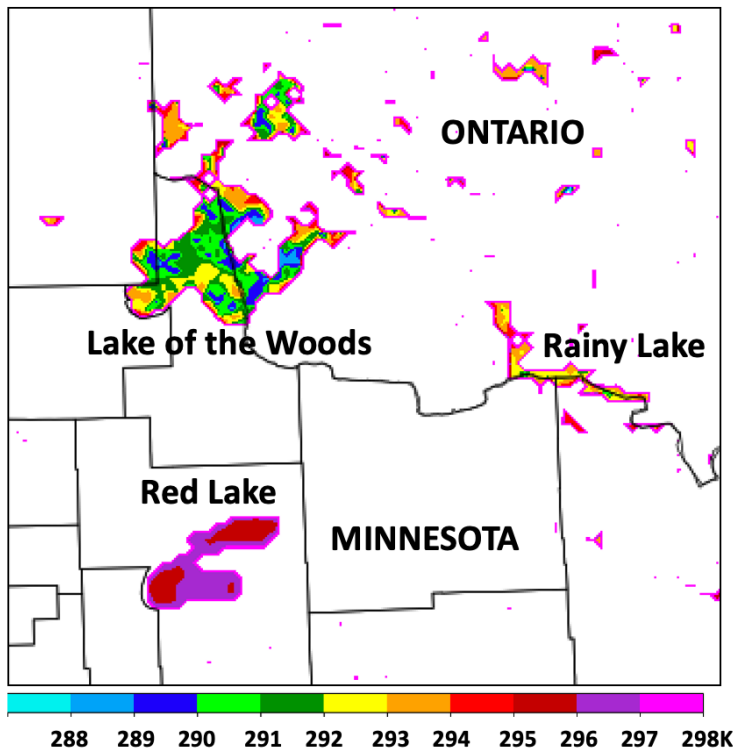


Fig. 9. HRRRv4-CLM lake surface temperature (K) for 1500 UTC 31 July 2021 for area over northern Minnesota (US) and southwestern Ontario (Canada).

Deleted: 9



Deleted:

[5]

Deleted: HRRR

The main deficiencies evident so far with the HRRR-CLM lake temperatures appear to be associated with errors in lake depth values. On the average, the current specified values for mean lake depth for most lakes are too deep compared to reality, since the preprocessing with the K12 dataset simply assigned a single lake depth value (maximum or mean) to all grid points for that lake even up to the modeled lake points adjacent to land, as shown in Table 5 for 16 or the 19 lakes studied. We also noted too-low lake temperatures in HRRRv4 for lake grid points at the western edge of a few lakes (e.g., Tahoe, Sebago (ME), Cayuga (NY), Champlain), all relatively deep lakes (Fig. 5, Table 5). We attribute this to 1-d upwelling from insufficient bathymetry data resulting in cylinder-like lake volumes with constant lake depths, therefore with a) too-deep lake-edge pixels coinciding with b) strong winds coming off from land areas with predominantly westerly winds. This deficient effect was not widespread for the HRRR model and did not affect the overall results. Again, this behavior is attributed to the behavior of the lake model over integrations with the inaccurate lake depth information and not to the lake cycling initialization design.

6 Conclusions

We report here on the first use of a small-lake model (CLM4.5, 10 layer) in US NOAA NWP models along with an ongoing cycling of lake temperatures since 2018 to initialize lake temperatures in each prediction. These models are the 3-km HRRRv4 (D22, J22) and 13-km RAPv5 hourly updated models, both of which became operational in December 2020 after cycling since August 2018. At 3-km grid spacing, the HRRR model applied this small-lake modeling and assimilation to 1864 small lakes varying in size from about 10 km² (single grid point) to 14 larger lakes over 1000 km² in surface area, but not including the Laurentian Great Lakes. The effectiveness of introducing the multi-layer lake model into the HRRR and RAP models was completely dependent on the initialization for lake temperatures. The introduction of a cycling capability through the hourly assimilation allowed the lake temperatures to evolve to accurate values, consistent with recent weather. In this paper, we describe the lake cycling applied for the NOAA regional 3-km HRRR and 13-km RAP weather models including the coupled 1-d CLM lake model. We also show some comparisons with other estimates of lake surface temperatures. From those comparisons, the cycled lake surface temperatures from the 3-km HRRR model were found to be reasonably accurate. HRRR lake surface temperatures were found to be generally within 1 K of in situ observations and within 2 K of the SPoRT estimates. Finally, NSST estimates of small-lake temperatures were found to often differ from in situ observations and HRRR estimates by 5-12 K. Other differences between lake-cycled HRRR estimates and SST-based estimates were up to 10-15 K.

From these initial results, we conclude that the lake-cycling initialization for small lakes has been effective overall, owing to accurate hourly estimates of near-surface temperature, moisture and winds, and shortwave and longwave estimates provided to

the 1-d CLM lake model every time step (20 s for 3-km HRRR model). The HRRR-CLM treatment also allows some inland lakes to freeze in winter, which is more consistent with observations. The lake cycling strategy is similar to that initialization method used by ECMWF for its 9-km (as of 2021) IFS (Integrated Forecast System) and using a binary lake mask in the 3-km HRRR model.

One deficiency noted was development of too-cold lake surface for a few lakes on their western boundary. We attribute this to the incorrect bathymetry data with constant lake depth (e.g., see caption for Table 5) causing an excessive 1-d upwelling from too-deep lake depth at western shores for these lakes. This issue is being addressed with a current project to improve lake bathymetry data for which results will be reported in the future. Also, HRRR-CLM cycling gave poorer results than NSST at least for Lake Pontchartrain (Lake #6 in Table 5), suggesting to use NSST for near-ocean lagoon areas. More investigation is needed for strong intralake variations overall in HRRR-CLM-cycling representation (e.g., Lake of the Woods in Fig. 9) and possible introduction of horizontal diffusion of temperature between adjacent lake points.

US NWS forecasters have reported much improved near-surface temperature and dewpoint predictions in the vicinity of small lakes from the 3-km HRRR model in 2021 since the implementation of the 1-d CLM lake model and lake-cycling initialization. Again, this effort complements the coupling of the HRRR model with the 3-d FVCOM hydrodynamical lake model for the Laurentian Great Lakes (Fujisaki-Manome et al, 2020) design to improve lake-effect snow predictions. These efforts are the most advanced lake-coupling and lake-initialization efforts at this point in US NOAA weather models.

Overall, the improved lake temperatures from the lake cycling initialization technique driven over a 3-year period by accurate atmospheric conditions described here results in improved fluxes of heat and moisture over using SST interpolation and improved nearby predictions of atmospheric 2 m temperature and 2 m moisture.

Code availability

This research used WRF version 3.9.1 including use of the option with the CLM lake model. All code is available from the National Center for Atmospheric Research (NCAR) at https://www2.mmm.ucar.edu/wrf/users/download/get_sources.html

Data availability

HRRR data (including lake surface temperature data under 'skin temperature' field) are publicly available via archives hosted by Amazon Web Services (<https://registry.opendata.aws/noaa-hrrr-pds/>) and Google Cloud Platform (<https://console.cloud.google.com/marketplace/product/noaa-public/hrrr?project=python-232920&pli=1>).

Author contributions

Deleted: Fukisaki

799 SB, TS, and EJ planned the design. TS and EJ carried out the actual coding for
800 modeling, data assimilation and scripts. EJ, SB, JK, and SK extracted data from
801 experiments and other sources. EJ and JK analyzed the results. SB wrote the
802 manuscript draft and led its revision. EA, AFM, JK, GM, AG and PC (along with TS and
803 EJ) reviewed and edited the manuscript.

804 **Acknowledgments**

805 Credit is due to the WRF model team at NCAR (Jimmy Dudhia) for their help in applying
806 the CLM lake model for the HRRR and RAP applications of the WRF model. We
807 greatly appreciate our NOAA colleague, Thomas Hamill (NOAA PSL), for Fig. 3 from
808 another already published article by him. We also thank Frank J. LaFontaine and Kevin
809 K. Fuell of the NASA SPoRT Team for providing archived Northern Hemisphere SST
810 composites. Thanks also to Rob Cifelli of NOAA/PSL for a very helpful review of our
811 manuscript. This work was supported by NOAA Research base funding.

812 **References**

- 813 Anderson, E. J., Fujisaki-Manome, A., Kessler, J., Lang, G. A., Chu, P. Y., Kelley, J. G.
814 W., et al.: Ice forecasting in the next-generation Great Lakes Operational Forecast
815 System (GLOFS). *Journal of Marine Science and Engineering*, 6(123),
816 <https://doi.org/10.3390/jmse6040123>, 2018
- 817 Balsamo, G., Salgado, R., Dutra, E., Boussetta, S., Stockdale, T., Potes, M.: On the
818 contribution of lakes in predicting near-surface temperature in a global weather
819 forecasting model. *Tellus A: Dynamic Meteorology and Oceanography*.
820 <https://doi.org/10.3402/tellusa.v64i0.15829>, 2012
- 821 Balsamo, G., Interactive lakes in the Integrated Forecast System. ECMWF Newsletter
822 137, p. 30-34. 10.21957/rffv1gir, 2013.
- 823
- 824 Balsamo, G., Mahfouf, J.-F.: Les schémas de surface continentale pour le suivi et la
825 prévision du système Terre au CEPMMT. *La Météorologie*, 108, 77-81, 2020.
- 826
- 827 Belovsky, G., Stephens, D., Perschon, C., et al.: The Great Salt Lake Ecosystem (Utah,
828 USA): long term data and a structural equation approach, *Ecosphere*, 2, 1-40,
829 doi.org/10.1890/ES10-00091.1, 2011.
- 830
- 831 Benjamin, S.G., D. Devenyi, S.S. Weygandt, K.J. Brundage, J.M. Brown, G. Grell, D.
832 Kim, B.E. Schwartz, T.G. Smirnova, T.L. Smith, G.S. Manikin: An hourly
833 assimilation/forecast cycle: the RUC. *Mon. Wea. Rev.*, 132, 495-518. 2004.
- 834 Benjamin, S.G., B.D. Jamison, W.R. Moninger, S. R. Sahm, B. Schwartz, T.W.
835 Schlatter: Relative short-range forecast impact from aircraft, profiler, radiosonde, VAD,
836 GPS-PW, METAR, and mesonet observations via the RUC hourly assimilation
837 cycle. *Mon. Wea. Rev.*, 138, 1319-1343. 2010.

Benjamin, S. G., S.S. Weygandt, M. Hu, C.A. Alexander, T.G. Smirnova, J.B. Olson, J.M. Brown, E. James, D.C. Dowell, G.A. Grell, H. Lin, S.E. Peckham, T.L. Smith, W.R. Moninger, G.S. Manikin: A North American hourly assimilation and model forecast cycle: The Rapid Refresh. *Mon. Wea. Rev.*, 144, 1669-1694. <http://dx.doi.org/10.1175/MWR-D-15-0242.1>. 2016.

Benjamin, S.G., E.P. James, M. Hu, C.R. Alexander, T.T. Ladwig, J.M. Brown, S.S. Weygandt, D.D. Turner, P. Minnis, W.L. Smith, Jr., and A. Heidinger: Stratiform cloud-hydrometeor assimilation for HRRR and RAP model short-range weather prediction. *Mon. Wea. Rev.*, 149, 2673-2694. <https://doi.org/10.1175/MWR-D-20-0319.1>. 2021.

Benjamin, S.G., T.G. Smirnova, E.P. James, L.-F. Lin, M. Hu, D.D. Turner, and S. He: Land-snow assimilation including a moderately coupled initialization method applied to NWP. *J. Hydromet.*, 23, 825-845, <https://doi.org/10.1175/JHM-D-21-0198.1>. 2022.

Boussetta, S.; Balsamo, G.; Arduini, G.; Dutra, E.; McNorton, J.; Choulga, M.; Agustí-Panareda, A.; Beljaars, A.; Wedi, N.; Muñoz-Sabater, J.; de Rosnay, P.; Sandu, I.; Hadade, I.; Carver, G.; Mazzetti, C.; Prudhomme, C.; Yamazaki, D.; Zsoter, E.: ECLand: The ECMWF Land Surface Modelling System. *Atmosphere*, 12, 723. <https://doi.org/10.3390/atmos12060723>, 2021.

Charusombat, U., Fujisaki-Manome, A., Gronewold, A. D., Lofgren, B. M., Anderson, E. J., Blanken, P. D., Spence, C., Lenters, J. D., Xiao, C., Fitzpatrick, L. E., and Cutrell, G.: Evaluating and improving modeled turbulent heat fluxes across the North American Great Lakes, *Hydrol. Earth Syst. Sci.*, 22, 5559–5578, <https://doi.org/10.5194/hess-22-5559-2018>, 2018.

Chen, C., Beardsley, R. C., & Cowles, G.: An unstructured grid, finite volume coastal ocean model (FVCOM) system. *Oceanography*, 19(1), 78–89. <https://doi.org/10.5670/oceanog.2006.92>, 2006.

Chen, C., Beardsley, R., Cowles, G., Qi, J., Lai, Z., Gao, G., et al.: An unstructured grid, Finite-Volume Coastal Ocean Model FVCOM -- User Manual. *Tech. Rep., SMAST/UMASSD-13-0701, Sch. for Mar. Sci. and Technol., Univ. of Mass. Dartmouth, New Bedford.*, 416 pp., 2013

Choulga, M., Kourzeneva, E., Balsamo, G., Boussetta, S., and Wedi, N.: Upgraded global mapping information for earth system modelling: an application to surface water depth at the ECMWF, *Hydrol. Earth Syst. Sci.*, 23, 4051–4076, <https://doi.org/10.5194/hess-23-4051-2019>, 2019.

De Pondeca, M.S.F.V., Manikin, G.S., DiMego, G., Benjamin, S.G., Parrish, D.F., Purser, R.J., Wu, W.-S., Horel, J.D., Myrick, D.T., Lin, Y., Aune, R.M., Keyser, D., Colman, B., Mann, G., and Vavra, J.: The Real-Time Mesoscale Analysis at NOAA's

880 National Centers for Environmental Prediction: Current status and development. *Wea.*
881 *Forecasting*, **26**, 593-612, <https://doi.org/10.1175/WAF-D-10-05037.1>, 2011

882

883 Dirmeyer, P.A., Halder, S., Bombardi, R.: On the harvest of predictability from land
884 states in a global forecast model. *J. Geophys. Res. Atmospheres*, **123**, 13,111-
885 13,127. <https://doi.org/10.1029/2018JD029103>, 2018.

886

899 Dowell, D. C., C. R. Alexander, E. P. James, S. S. Weygandt, S. G. Benjamin, G. S.
900 Manikin, B. T. Blake, J. M. Brown, J. B. Olson, M. Hu, T. G. Smirnova, T. Ladwig, J. S.
901 Kenyon, R. Ahmadov, D. D. Turner, [J. D. Duda](#), and T. I. Alcott: The High-Resolution
902 Rapid Refresh (HRRR): An hourly updating convection-allowing forecast model. Part I:
903 Motivation and system description. *Wea. Forecasting*, **150**,
904 <https://doi.org/10.1175/WAF-D-21-0151.1>. 2022.

905 Downing, J.A. et al: The global abundance and size distribution of lakes, ponds, and
906 impoundments. *Limnol. Oceanogr.*, **51**, 2388-2397. 2006.

907

908 Dutra, E, Stepanenko, V. M, Balsamo, G, Viterbo, P, Miranda, P. M and co-authors: An
909 offline study of the impact of lakes on the performance of the ECMWF surface scheme.
910 *Boreal Env. Res.* **15**, 100–112, 2010.

911

912 ECMWF, OpenIFS: Lakes,
913 <https://confluence.ecmwf.int/display/OIFS/3.5+OpenIFS:+Lakes>. Accessed 7 Dec 2021,
914 2020.

915

916 Fiedler, E.K., Martin, M.J., Roberts-Jones, J.: An operational analysis of Lake Surface
917 Water Temperature. *Tellus A*, **6**, <https://doi.org/10.3402/tellusa.v66.21247>, 2014.

918

919 Fujisaki-Manome, A., G. E. Mann, E. J. Anderson, P. Y. Chu, L. E. Fitzpatrick, S. G.
920 Benjamin, E. P. James, T. G. Smirnova, C. R. Alexander, and D. M. Wright:
921 Improvements to lake-effect snow forecasts using a one-way air-lake model coupling
922 approach. *J. Hydrometeor.*, **21**, 2813-2828, <https://doi.org/10.1175/JHM-D-20-0079.1>,
923 2020.

924

925 Gao, G., C. Chen, J. Qi, and R. C. Beardsley: An unstructured-grid, finite-volume sea
926 ice model: Development, validation, and application. *J. Geophys.*
927 *Res.*, **116**, C00D04, <https://doi.org/10.1029/2010JC006688>. 2011.

928

929 Gemmill, W., B. Katz, and X. Li: Daily real-time, global sea surface temperature—High-
930 resolution analysis: RTG_SST_HR. NCEP Office Tech. Note 260, 39 pp. Available
931 online at <http://polar.ncep.noaa.gov/mmab/papers/tn260/MMAB260.pdf> , 2007.

932

933 Gu, H., Jin, J., Wu, Y., Ek, M.B., and Subin, Z.M.: Calibration and validation of lake
934 surface temperature simulations with the coupled WRF-lake model. *Climatic Change*,
935 **129**, 471-483. DOI 10.1007/s10584-013-0978-y, 2015.

936
 937 Hamill, T.M.: Benchmarking the raw model-generated background forecast in rapidly
 938 updated surface temperature analyses. Part I: Stations. *Mon. Wea. Rev.*, **148**, 689-
 939 700. <https://doi.org/10.1175/MWR-D-19-0027.1>, 2020.
 940
 941 Hostetler, S.W., Bates, G., Giorgi, F.: Interactive coupling of a lake thermal model with
 942 a regional climate model. *J. Geophys. Res.*, **98**, 5045-5057. DOI:[10.1029/92JD02843](https://doi.org/10.1029/92JD02843),
 943 1993.
 944
 945 Hunter, T. S., Clites, A. H., Campbell, K. B., & Gronewold, A. D.: Development and
 946 application of a monthly hydrometeorological database for the North American Great
 947 Lakes - Part I: precipitation, evaporation, runoff, and air temperature. *Journal of Great
 Lakes Research*, **41**(1), 65–77, 2015
 948
 949 James, E. P., and S. G. Benjamin: Observation system experiments with the hourly
 950 updating Rapid Refresh model using GSI hybrid ensemble-variational data
 951 assimilation. *Mon. Wea. Rev.*, **145**(8), 2897-2918. [https://doi.org/10.1175/MWR-D-16-](https://doi.org/10.1175/MWR-D-16-0398.1)
 952 [0398.1](https://doi.org/10.1175/MWR-D-16-0398.1), 2017.
 953
 954 James, E. P., C. R. Alexander, D. C. Dowell, S. S. Weygandt, S. G. Benjamin, G. S.
 955 Manikin, J. M. Brown, J. B. Olson, M. Hu, T. G. Smirnova, T. Ladwig, J. S. Kenyon, and
 956 D. D. Turner: The High-Resolution Rapid Refresh (HRRR): An hourly updating
 957 convection-allowing forecast model. Part II: Forecast performance. *Wea. Forecasting*,
 958 **150**, <https://doi.org/10.1175/WAF-D-21-0130.1>, 2022.
 959
 960 Kelley, S.G.T, J.G.W. Kelley, and E.J. Anderson: Evaluation of the NASA SPoRT
 961 Composite Product of surface water temperatures for large lakes in New England and
 962 New York State. *Abstract, 24th Conference on Satellite Meteorology, Oceanography,
 963 and Climatology*. Available at
 964 <https://ams.confex.com/ams/101ANNUAL/meetingapp.cgi/Paper/381301>, 2021.
 965
 966 Kourzeneva, E., Martin, E., Batrak, Y., LeMoigne, P. Faroux: Climate data for
 967 parameterisation of lakes in Numerical Weather Prediction models, *Tellus A.*, **64**: . DOI:
 968 [10.3402/tellusa.v64i0.17226](https://doi.org/10.3402/tellusa.v64i0.17226), 2012a.
 969
 970 Kourzeneva, E., Asensio, H., Martin, E., Faroux: Global gridded dataset of lake
 971 coverage and lake depth for use in numerical weather prediction and climate modelling.
 972 *Tellus A.*, **64**: 15640. [10.3402/tellusa.v64i0.15640](https://doi.org/10.3402/tellusa.v64i0.15640), 2012b.
 973
 974 Lawrence, D. M., Fisher, R. A., Koven, C. D., Oleson, K. W., Swenson, S. C., Bonan,
 975 G., et al.: The Community Land Model version 5: Description of new features,
 976 benchmarking, and impact of forcing uncertainty. *Journal of Advances in Modeling Earth
 977 Systems*, **11**, 4245-4287. <https://doi.org/10.1029/2018MS001583>, 2019.

978 Lewis, W. M., Jr.: A revised classification of lakes based on mixing. *Can. J. Fish.*
 979 *Aquat. Sci.* 40, 1779-1787. <https://doi.org/10.1139/f83-207>, 1983
 980
 981 Mallard, M.S., Nolte, C.G., Spero, T.L., Bullock, O.R., Alapaty, K., Herwehe, J.A., Gula,
 982 J., Bowden, J.H.: Technical challenges and solutions in representing lakes when using
 983 WRF in downscaling applications. *Geosci. Model Dev.*, 8, 1085-1096, 2015.
 984
 985 Mironov, D., Heise, E., Kourzeneva, E., Ritter, B., Schneider, N., and Terzhevik, A.:
 986 Implementation of the lake parameterisation scheme Flake into numerical weather
 987 prediction model COSMO, *Boreal Environ. Res.*, 15, 218–230, 2010.
 988
 989 Muñoz-Sabater, J., H. Lawrence, C. Albergel, P. de Rosnay, L. Isaksen, S.
 990 Mecklenburg, Y. Kerr, and M. Drusch: Assimilation of SMOS brightness temperatures in
 991 the ECMWF Integrated Forecasting System. *Quart. J. Roy. Meteor. Soc.*, **145**, 2524–
 992 2548, <https://doi.org/10.1002/QJ.3577> , 2019.
 993
 994 NASA: Surface water temperature composite.
 995 <https://weather.msfc.nasa.gov/sport/sst/>. Downloaded 2 Nov 2021, 2021
 996
 997 National Weather Service: Service Change Notice 20-10. Available at
 998 https://www.weather.gov/media/notification/scn20-10nsst1_0.pdf , 2020.
 999
 1000 Pondeva, M.S.F.V. de, G.S. Manikin, G. DiMego, S.G. Benjamin, D.F. Parrish, R.J.
 1001 Purser, W.-S. Wu, J. Horel, Y. Lin, R.M. Aune, D. Keyser, L. Anderson, B. Colman, G.
 1002 Mann, and J. Vavra: The Real-Time Mesoscale Analysis at NOAA's National Centers
 for Environmental Prediction: Current Status and Development. *Wea. Forecasting*, **26**,
 593-612. 2011.
 1003
 1004 Powers, J. G., and Coauthors: The Weather Research and Forecasting Model:
 1005 Overview, system efforts, and future directions. *Bull. Amer. Meteor. Soc.*, **98**, 1717-
 1006 1737, <https://doi.org/10.1175/BAMS-D-15-00308.1>, 2017
 1007
 1008 Railsback, B.: Some fundamentals of mineralogy and geochemistry. Figure on lake
 1009 salinity at <http://railsback.org/Fundamentals/SFMGLakeSize&Salinity07I.pdf>, 2006
 1010
 1011 Skamarock, W. C., and Coauthors, 2019: A description of the Advanced Research WRF
 1012 version 4. NCAR Tech. Note NCAR/TN-556+STR, 162 pp., [Available online at
 1013 http://www2.mmm.ucar.edu/wrf/users/docs/technote/v4_technote.pdf]. 2019.
 1014
 1015 Subin, Z. M., Riley, W. J., & Mironov, D.: An improved lake model for climate
 1016 simulations: Model structure, evaluation, and sensitivity analyses in CESM1. *Journal of*
 1017 *Advances in Modeling Earth Systems*, 4(1). <https://doi.org/10.1029/2011ms000072>,
 1018 2012.

1019 Thiery, W., Stepanenko, V., Fang, X., Jöhnk, D., Li, Z., Martynov, A., Perroud, M.,
 1020 Subin, Z., Darchambeau, F., Mironov, D., Van Lipzig, N.: LakeMIP Kivu: evaluating the
 1021 representation of a large, deep tropical lake by a set of one-dimensional lake models,
 1022 *Tellus A: Dynamic Meteorology and Oceanography*, 66:1, 21390, DOI:
 1023 10.3402/tellusa.v66.21390, 2014.
 1024

1025 U.S. National Ice Center, updated daily: *IMS Daily Northern Hemisphere Snow and Ice*
 1026 *Analysis at 1 km, 4 km, and 24 km Resolutions, Version 1*. Boulder, Colorado USA.
 1027 NSIDC: National Snow and Ice Data Center.
 1028 Doi: <https://doi.org/10.7265/N52R3PMC>. Accessed 8 November 2021, 2021.
 1029

1030 Vanderkelen, I., van Lipzig, N. P. M., Sacks, W. J., Lawrence, D. M., Clark, M.,
 1031 Mizukami, N., Pokhrel, Y., and Thiery, W.: The impact of global reservoir expansion on
 1032 the present-day climate, EGU General Assembly 2021, online, 19–30 Apr 2021,
 1033 EGU21-723, <https://doi.org/10.5194/egusphere-egu21-723>, 2021
 1034

1035 Verpoorter, C., Kutser, T., Seekell, D.A., and Tranvik. L.J.: A global inventory of lakes
 1036 based on high-resolution satellite imagery. *Geophys. Res. Lett.*, 41, 6396–6402,
 1037 doi:10.1002/2014GL060641. 2014.
 1038

1039 Wang, F., Ni, G., Riley, W. J., Tang, J., Zhu, D., and Sun, T.: Evaluation of the WRF
 1040 lake module (v1.0) and its improvements at a deep reservoir, *Geosci. Model Dev.*, 12,
 1041 2119–2138, <https://doi.org/10.5194/gmd-12-2119-2019>, 2019.
 1042

1043 Weygandt, S. S., S. G. Benjamin, M. Hu, C. R. Alexander, T. G. Smirnova, and E. P.
 1044 James: Radar reflectivity-based model initialization using specified latent heating
 1045 (Radar-LHI) within a diabatic digital filter or pre-forecast integration. *Wea. Forecasting*,
 1046 150, <https://doi.org/10.1175/WAF-D-21-0142.1>, 2022.
 1047

1048 Wilson, R. C., Hook, S. J., Schneider, P., and Schladow, S. G.: Skin and bulk
 1049 temperature difference at Lake Tahoe: A case study on lake skin effect. *J. Geophys.*
 1050 *Res. Atmos.*, 118, 10,332-10,346, <https://doi.org/10.1002/jgrd.50786>, 2013.

Deleted: Forecasting, 150,
<https://doi.org/10.1175/WAF-D-21-0130.1>,

Page 12: [1] Deleted	Stan Benjamin	7/28/22 11:43:00 AM
----------------------	---------------	---------------------

Page 16: [2] Deleted	Stan Benjamin	7/28/22 11:43:00 AM
----------------------	---------------	---------------------

Page 17: [3] Deleted	Stan Benjamin	7/28/22 11:43:00 AM
----------------------	---------------	---------------------

Page 22: [4] Deleted	Stan Benjamin	7/28/22 11:43:00 AM
----------------------	---------------	---------------------

Page 24: [5] Deleted	Stan Benjamin	7/28/22 11:43:00 AM
----------------------	---------------	---------------------